A NOVEL WIDE-STOPBAND BANDSTOP FILTER WITH SHARP-REJECTION CHARACTERISTIC AND ANALYTICAL THEORY

Liming Liang, Yuanan Liu, Jiuchao Li[*]**, Shulan Li, Cuiping Yu, Yongle Wu, and Ming Su**

School of Electronic Engineering, Beijing University of Posts and Telecommunications, Beijing, China

Abstract—A novel bandstop filter with wide-stopband performance is proposed and discussed in this paper. This circuit configuration includes two-section coupled lines and three open-circuit transmission-line stubs. Due to the symmetry of this proposed structure, closed-form equations for scattering parameters are investigated. Transmission zeros and poles location for different circuit parameters are discussed, and the corresponding design curves are given. In order to verify this new filter circuit structure and its corresponding design theory, several typical numerical examples are designed, calculated and illustrated. Furthermore, a practical wideband bandstop filter with $-20\,\mathrm{dB}$ fractional bandwidth of 94% centered at 3 GHz with sharp rejection characteristics is fabricated to validate the theoretical prediction. The measured frequency response of the filter agrees excellently with the predicted result.

1. INTRODUCTION

Microstrip planar-circuit filters play an important role in the design of Microwave or RF subsystem. Recently, various filters with different features [1–12] have been researched widely. As significant circuit component in microwave system, the band-stop filter is usually used to reject undesired frequency band located within the useful passband. The design problem of a wideband BSF using conventional [13] and optimum [14] designs arises from the fabrication limit of high impedance lines required for the connecting lines of shunt open-stubs.

Recently, the signal interference technique has been proposed to design a wideband BSF with high skirt selectivity [15, 16]. In [15], two parallel transmission lines of different electrical lengths and characteristic impedances are used for signal interference. This structure produce two transmission zeros. Sharp rejection characteristic can be obtained by placing these zeros near the stopband edges. Further, two shunt open-stubs are used to improve the stopband rejection level. In this procedure, the stopband rejection level is limited by the fabrication limit of a high impedance line. Also the maximum achievable separation between the zeros is 66.67%. In [16], a modified transmission line configuration is proposed to increase this theoretical limit of maximum zero separation. This new configuration can provide a fractional bandwidth more than double of that reported in [15]. In addition to signal interference technology, anti-coupled line, as a new circuit configuration, is also often used to design compact and wideband bandstop filters [17–21]. In [17], a compact parallel-coupled transmission line section, connected at their both ends, is proposed to obtain as much as five transmission zeros. These zeros can be arranged to design a sharp rejection wideband bandstop filter (BSF). In [18], a compact unit of parallel coupled transmission line is adopted to design a compact, sharp-rejection, wideband bandstop filter (BSF). The rejection depth and bandwidth can be easily controlled by the coupled-line parameters. In [19], a compact wideband high-rejection microstrip bandstop filter using two meandered parallel-coupled lines of different electrical lengths and characteristic impedances in shunt is presented. The transmission and reflection zeros of the filter can be controlled through analytical equations and rulers given. In [20], this paper proposes and discusses a novel band-stop filter with wide upper pass-band performance. Due to using three-section transimission-line stubs and coupled-line section, this filter not only features good band-stop filtering property, but also has wide upper pass-band. In [21], a novel one-section bandstop filter (BSF), which possesses the characteristics of compact size, wide bandwidth, and low insertion loss is proposed and fabricated. This bandstop filter was constructed by using single quarter-wavelength resonator with one section of anti-coupled lines with short circuits at one end.

In this paper, a new coupled-line circuit is proposed to construct a novel bandstop filter. This investigated circuit configuration is composed of two-section coupled lines and three open-circuit transmission-line stubs. Since the total circuit layout is based on coupled lines, which is symmetrical and simple, this BSF not only has analytical scattering parameters' expressions, but also features compact size and flexible reconfiguration. Furthermore, based on

the obtained equations, the design curves for transmission zeros and poles location are illustrated when different circuit parameters are adopted. Then, several numerical examples are presented for theoretical verifications. In addition, a practical wideband bandstop filter with $-20\,\mathrm{dB}$ fractional bandwidth of 94% centered at $3\,\mathrm{GHz}$ with sharp rejection characteristics is fabricated to validate the theoretical prediction. The measured frequency response of the filter agrees excellently with the predicted result.

2. THE CIRCUIT STRUCTURE AND THEORY OF THE PROPOSED BAND-STOP FILTER

The proposed BSF's circuit structure is illustrated in Fig. 1. This novel structure consists of two-section coupled lines (Z_{ie}, Z_{io}, $i = 2$, 3) and three open-circuit transmission-line stubs,. One open-circuit stub is connected at the point A (Z_4), while another two open-circuit stubs are symmetrically connected to both ends of the coupled line (Z_1), as shown in Fig. 1. Two port impedances are chosen as Z_0. Since the total circuit configuration shown in Fig. 1 is symmetrical, this model's scattering parameter can be analyzed through the even- and odd-mode method. Figs. 2(a) and (b) show the even- and odd-mode equivalent circuits of the total circuit configuration in Fig. 1, respectively.
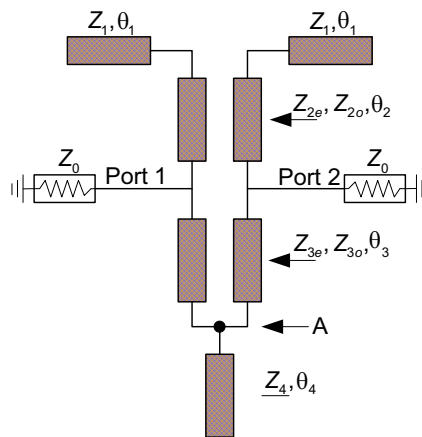

Figure 1. The proposed circuit structure of a novel bandstop filter.

According to the symmetrical network analysis results [1], the network analysis of Fig. 1 will be simplified by analyzing the one-port networks shown in Figs. 2(a) and (b). In other words, if the one-port
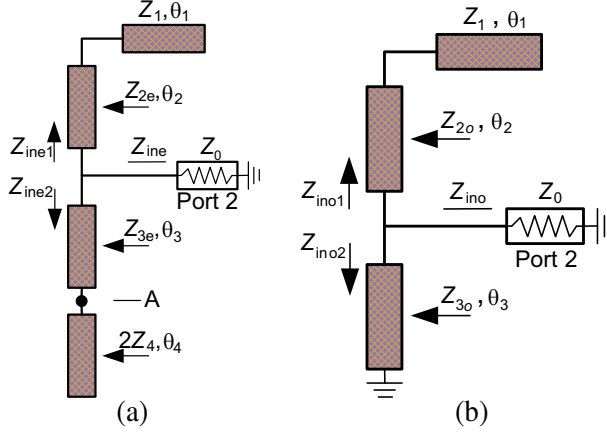
Figure 2. The equivalent simplified circuit structures of the bandstop filter. (a) Even-mode analysis. (b) Odd-mode analysis.

even- and odd-mode scattering parameters S_{11e} and S_{11o} are obtained, the two-port scattering parameters of Fig. 1 can be calculated as:

$$S_{11} = \frac{S_{11e} + S_{11o}}{2}, \quad S_{21} = \frac{S_{11e} - S_{11o}}{2} \tag{1}$$

Two groups of input equivalent impedances including: Z_{ine}, Z_{ine1}, Z_{ine2}, Z_{ino}, Z_{ino1}, Z_{ino2} are defined in the Figs. 2(a) and (b). For Fig. 2(a), their mathematical expressions can be obtained as:

$$Z_{ine1} = \frac{jZ_{2e}\left(Z_{2e}\tan\theta_1\tan\theta_2 - Z_1\right)}{Z_{2e}\tan\theta_1 + Z_1\tan\theta_2} \tag{2a}$$

$$Z_{ine2} = \frac{jZ_{3e}\left(Z_{3e}\tan\theta_3\tan\theta_4 - 2Z_4\right)}{Z_{3e}\tan\theta_4 + 2Z_4\tan\theta_3} \tag{2b}$$

The total input equivalent impedance Z_{ine} is calculated by using the following equation:

$$Z_{ine} = \frac{Z_{ine1}Z_{ine2}}{Z_{ine1} + Z_{ine2}} \tag{3a}$$

Thus, the final result is expressed by:

$$Z_{ine} = \frac{jZ_{2e}Z_{3e}\left(\begin{array}{l}[\tan\theta_1\tan\theta_2\left(Z_{2e}Z_{3e}\tan\theta_3\tan\theta_4 - 2Z_{2e}Z_4\right)\\ - \left(Z_1Z_{3e}\tan\theta_3\tan\theta_4 - 2Z_1Z_4\right)]\end{array}\right)}{\left(\begin{array}{l}Z_{2e}Z_{2e}\tan\theta_1\tan\theta_2\left(2Z_4\tan\theta_3 + Z_{3e}\tan\theta_4\right)\\ + Z_{3e}Z_{3e}\tan\theta_3\tan\theta_4\left(Z_{2e}\tan\theta_1 + Z_1\tan\theta_2\right)\\ - Z_{2e}Z_{3e}\left(2Z_4\tan\theta_1 + Z_1\tan\theta_4\right)\\ - 2Z_1Z_4\left(Z_{2e}\tan\theta_3 + Z_{3e}\tan\theta_2\right)\end{array}\right)} \tag{3b}$$

Similarly, for Fig. 2(b), the odd-mode input equivalent impedances can be derived as:

$$Z_{ino1} = \frac{jZ_{2o}\left(Z_{2o}\tan\theta_1\tan\theta_2 - Z_1\right)}{Z_{2o}\tan\theta_1 + Z_1\tan\theta_2} \tag{4a}$$

$$Z_{ino2} = jZ_{3o}\tan\theta_3 \tag{4b}$$

The final odd-mode input impedance Z_{ino} can be obtained as:

$$\begin{cases} Z_{ino} = \dfrac{Z_{ino1}Z_{ino2}}{Z_{ino1} + Z_{ino2}} \\[2mm] \begin{aligned} Z_{ino} = \dfrac{jZ_{2o}Z_{3o}\tan\theta_3(Z_{2o}\tan\theta_1\tan\theta_2 - Z_1)}{\begin{array}{c} Z_{2o}\tan\theta_1(Z_{2o}\tan\theta_2 + Z_{3o}\tan\theta_3) \\ + Z_1(Z_{3o}\tan\theta_2\tan\theta_3 - Z_{2o}) \end{array}} \end{aligned} \end{cases} \tag{5}$$

Then, the even-mode and odd-mode scattering parameters of this proposed bandstop filter can be calculated by:

$$S_{11e} = \frac{Z_{ine} - Z_0}{Z_{ine} + Z_0} \tag{6a}$$

$$S_{11o} = \frac{Z_{ino} - Z_0}{Z_{ino} + Z_0} \tag{6b}$$

When the above Equations (1)–(6) are applied and the symmetrical property is considered, the external scattering parameters can be expressed by:

$$S_{11} = S_{22} = \frac{S_{11e} + S_{11o}}{2} \tag{7a}$$

$$S_{21} = S_{12} = \frac{S_{11e} - S_{11o}}{2} \tag{7b}$$

By combining (6) and (7), the mathematical expressions of scattering parameters are:

$$S_{11} = \frac{Z_{ine}Z_{ino} - Z_0^2}{\left(Z_{ine} + Z_0\right)\left(Z_{ino} + Z_0\right)} \tag{8a}$$

$$S_{21} = \frac{Z_0\left(Z_{ine} - Z_{ino}\right)}{\left(Z_{ine} + Z_0\right)\left(Z_{ino} + Z_0\right)} \tag{8b}$$

Obviously, there is a rigorous mathematical relationship that $S_{21} = 0$ at the operating frequency in ideal bandstop filters. Furthermore, the following expression can be achieved from (8b):

$$Z_{ine} - Z_{ino} = 0 \tag{9}$$

The final Equation (10) including the characteristic impedances and electrical lengths is:

$$\left\{ Z_{2e}Z_{3e} \begin{bmatrix} \tan\theta_1 \tan\theta_2 \left(Z_{2e}Z_{3e}\tan\theta_3\tan\theta_4 - 2Z_{2e}Z_4 \right) \\ - \left(Z_1 Z_{3e}\tan\theta_3\tan\theta_4 - 2Z_1 Z_4 \right) \end{bmatrix} \right\}$$

$$\times \left\{ \begin{matrix} Z_{2o}\tan\theta_1 \left(Z_{2o}\tan\theta_2 + Z_{3o}\tan\theta_3 \right) \\ + Z_1 \left(Z_{3o}\tan\theta_2 \tan\theta_3 - Z_{2o} \right) \end{matrix} \right\}$$

$$= \left\{ \begin{matrix} Z_{2e}Z_{2e}\tan\theta_1\tan\theta_2 \left(2Z_4\tan\theta_3 + Z_{3e}\tan\theta_4 \right) \\ + Z_{3e}Z_{3e}\tan\theta_3\tan\theta_4 \left(Z_{2e}\tan\theta_1 + Z_1\tan\theta_2 \right) \\ - Z_{2e}Z_{3e} \left(2Z_4\tan\theta_1 + Z_1\tan\theta_4 \right) \\ - 2Z_1 Z_4 \left(Z_{2e}\tan\theta_3 + Z_{3e}\tan\theta_2 \right) \end{matrix} \right\}$$

$$\times \left\{ Z_{2o}Z_{3o}\tan\theta_3 \left(Z_{2o}\tan\theta_1\tan\theta_2 - Z_1 \right) \right\} \qquad (10)$$

Therefore, according to the analytical Equations (1)–(8), we can calculate and analyze the external scattering parameters performance (including magnitude and phase information) of this novel bandstop filter. The bandstop performance at the operating frequency is determined by the mathematical Equation (10).

3. CHARACTERISTIC OF THE PROPOSED BANDSTOP FILTER

An ideal bandstop filter property can be described by using the rigorous relationships including $S_{11} = 0$ for out of band and $S_{21} = 0$ for in-band. The condition of transmission zeros can be obtained when $S_{21} = 0$. Further, the condition of reflection zeros can be obtained when $S_{11} = 0$. Based on the number of transmission zeros, Bandstop filter can be divided into two types, as Case A and Case B.

3.1. Case A ($\theta_1 = 90$; $\theta_2 = 90$; $\theta_3 = 90$; $\theta_4 = 90$ Degrees)

In the following numerical and experimental examples, electrical lengths of coupled lines and transmission lines are all specified at 3 GHz. Furthermore, we define five special frequencies including f_{p1}, f_{p2}, f_{z1}, f_{z2}, f_{z3}. The frequency point f_{pi} ($i = 1$, 2) is the ith reflection zeros in the low frequency pass band and its value will be nonzero. The frequency point f_{zi} ($i = 1$, 2, 3) corresponds to the ith transmission zeros. For clarity, the illustration about these five special frequencies

will be presented in the simulated scattering parameters (Example A in Fig. 5).

Figure 3 shows the performance variation of this proposed BSF when different electrical characteristic impedances are adopted. As shown in Figs. 3(b) and (d), the frequency point f_{z3} significantly decreases as Z_{2e} and Z_{3e} increases. However, the reverse phenomenon can be observed in Figs. 3(c) and (e). In addition, it can be seen from Fig. 3(a) that f_{z3} slightly declines as Z_1 increases. Totally, the variation trend for f_{p1}, f_{p2}, and f_{z1} is not obvious in Figs. 3(a)–(f). From Figs. 3(c), (e), and (f), we can see that f_{z2} slightly decreases as Z_{2o}, Z_{3o}, and Z_4 increases. Similarly, the reverse phenomenon can be observed in Figs. 3(a), (b), and (d). Through the above analysis, we can find that the location of transmission zeros (f_{z1}, f_{z2}, f_{z3}) can be changed of varying degrees by adjusting electrical characteristic impedances (Z_1, Z_{2e}, Z_{2o}, Z_{3e}, Z_{3o}, Z_4).

Figure 4 shows the variation of Transition-Band Slope and 20 dB Attenuation Bandwidth for different electrical characteristic impedances. First, we give the definition of these two parameters. At transition-band between passband and stopband, we define two frequencies, as $f_1 = 1.42\,\text{GHz}$ and $f_2 = 1.43\,\text{GHz}$. α_1 (dB) and α_2 (dB) are the amount of attenuation at f_1 and f_2, respectively. So Transition-Band Slope (dB/GHz) is derived as:

$$slope = \frac{\alpha_2 - \alpha_1}{f_2 - f_1} = 100 \times (\alpha_2 - \alpha_1) \text{ dB/GHz} \tag{11}$$

The 20 dB Attenuation Bandwidth is defined as:

$$\Delta_{20\,\text{dB}} = \frac{f_H^{20\,\text{dB}} - f_L^{20\,\text{dB}}}{f_0} \times 100\% \tag{12}$$

where $f_H^{20\,\text{dB}}$ and $f_L^{20\,\text{dB}}$ are the upper frequency and the lower

Table 1. The electrical parameters' values for Figs. 3 and 4 ($Z_0 = 50\,\text{Ohm}$).

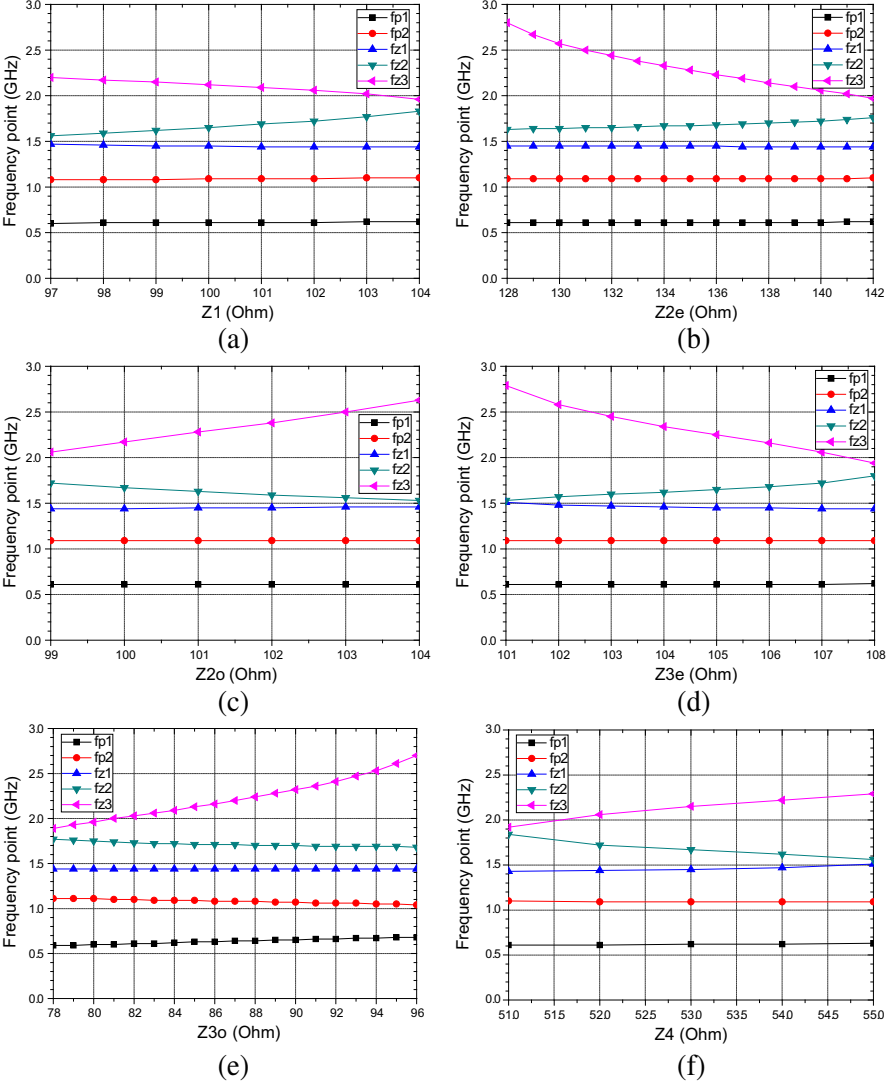| Figures	Fig. 3 (a) and Fig. 4(a)	(b)	(c)	(d)	(e)	(f)
Z_1 (Ohm)	$97 \sim 104$	102	102	102	102	102
Z_{2e}	140	$128 \sim 142$	140	140	140	140
Z_{2o}	99	99	$99 \sim 104$	99	99	99
Z_{3e}	107	107	107	$101 \sim 108$	107	107
Z_{3o}	83	83	83	83	$78 \sim 96$	83
Z_4	52	52	52	52	52	$51 \sim 55$

Figure 3. The defined frequency points **vs** different electrical parameters including (a) Z_1, (b) Z_{2e}, (c) Z_{2o}, (d) Z_{3e}, (e) Z_{3o}, (f) Z_4.

frequency of the stopband at 20 dB attenuation, respectively. f_0 is the center frequency.

From Figs. 3(a)–(f), we can see that BW2020 dB nearly has no variation. However, as shown in Fig. 4(b), slope changes irregularly and has relatively large fluctuation as Z_{2e} increases. The frequency point f_{z3} significantly decreases as Z_{2e} and Z_{3e} increases. In addition,
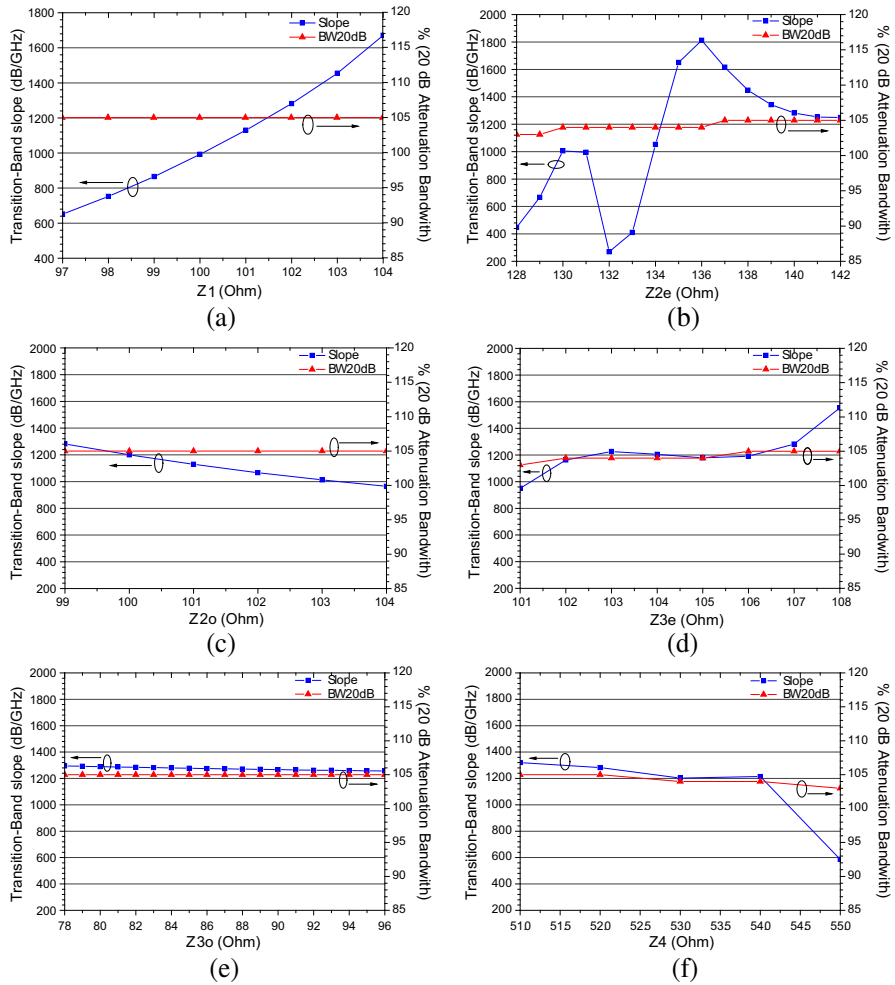
Figure 4. The defined transition-band slope and 20 dB attenuation bandwidth **vs** different electrical parameters including (a) Z_1, (b) Z_{2e}, (c) Z_{2o}, (d) Z_{3e}, (e) Z_{3o}, (f) Z_4.

it can be seen from Fig. 4(a) that the slope significantly declines as Z_1 increases.

Since different electrical parameters respond to different special frequency points f_{p1}, f_{p2}, f_{z1}, f_{z2}, and f_{z3}, also different BW20 dB and slope, it is very difficult to determinate a unique design synthesis method for this novel BSF. The chosen electrical parameters for Figs. 3 and 4 are listed in Table 1.
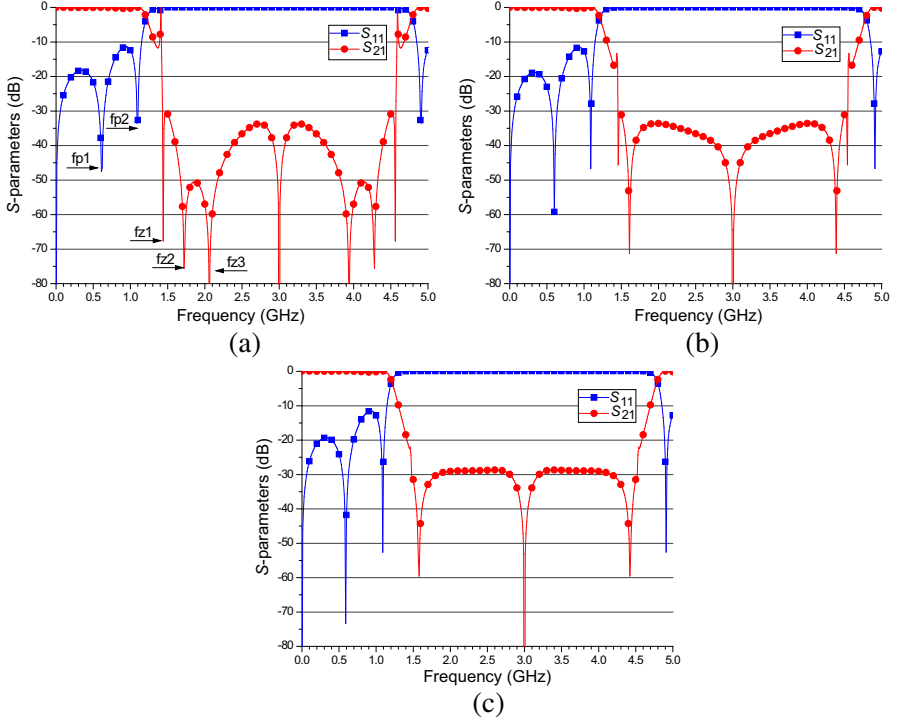
Figure 5. The simulated scattering parameters of filters of case A. (a) With $Z_1 = 102\,\Omega$, $Z_{2e} = 140\,\Omega$, $Z_{2o} = 99\,\Omega$, $Z_{3e} = 107\,\Omega$, $Z_{3o} = 83\,\Omega$, $Z_4 = 52\,\Omega$, (b) with $Z_1 = 102\,\Omega$, $Z_{2e} = 123\,\Omega$, $Z_{2o} = 99\,\Omega$, $Z_{3e} = 107\,\Omega$, $Z_{3o} = 83\,\Omega$, $Z_4 = 52\,\Omega$, (c) with $Z_1 = 102\,\Omega$, $Z_{2e} = 113\,\Omega$, $Z_{2o} = 99\,\Omega$, $Z_{3e} = 107\,\Omega$, $Z_{3o} = 83\,\Omega$, $Z_4 = 52\,\Omega$.

For case A, three numerical examples are designed and calculated. The achieved simulated results shown in Fig. 5 are based on ideal and lossless coupled-line and transmission-line circuit models. This type of filter can achieve seven, five and three transmission zeros when selecting different electrical characteristic impedances, as shown in Figs. 5(a), (b), and (c).

3.2. Case B ($\theta_1 = 180$; $\theta_2 = 180$; $\theta_3 = 90$; $\theta_4 = 90$ Degrees)

Figure 6 shows the circuit transmission responses for Case B. The achieved simulated results shown in Fig. 6 are also based on ideal and lossless coupled-line and transmission-line circuit models. For this type of filter, we can only get three or one transmission zeros for different electrical characteristic impedances, different from Case A that can achieve up to seven transmission zeros.

4. SIMULATED AND MEASURED EXAMPLES

In order to experimentally verify the proposed bandstop filter, a prototype filter (Case A) is designed, fabricated, and measured. This typical and ideal filter has the following electrical parameters: $Z_1 = 102\,\Omega$, $Z_{2e} = 140\,\Omega$, $Z_{2o} = 99\,\Omega$, $Z_{3e} = 107\,\Omega$, $Z_{3o} = 83\,\Omega$, $Z_4 = 52\,\Omega$. Based on the lossless transmission-line and coupled-line models, the calculated scattering parameters are shown in Fig. 5(a). This ideal filter operates at $3\,\mathrm{GHz}$. The $-20\,\mathrm{dB}$ bandstop fractional bandwidth is about 106% ($1.43\,\mathrm{GHz}$–$4.57\,\mathrm{GHz}$). The Transition-Band Slope is $1282\,\mathrm{dB/GHz}$ (simulated attenuations being 14.225 and 27.044 dB at 1.42 and $1.43\,\mathrm{GHz}$). The lower $10\,\mathrm{dB}$ return-loss pass-band is from DC to $1.15\,\mathrm{GHz}$ while the upper $10\,\mathrm{dB}$ return-loss pass-band is from 4.85 to $5\,\mathrm{GHz}$. The lower pass-band insertion loss is within $1\,\mathrm{dB}$ up to $1.17\,\mathrm{GHz}$.
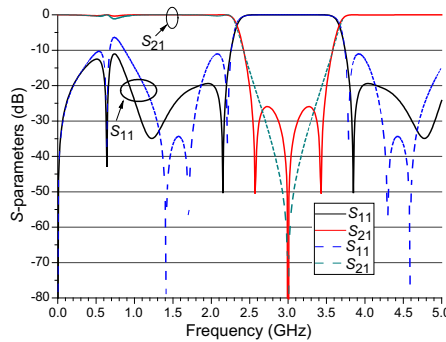

Figure 6. The simulated scattering parameters of filters of case B. — with $Z_1 = 96\,\Omega$, $Z_{2e} = 158\,\Omega$, $Z_{2o} = 60\,\Omega$, $Z_{3e} = 122\,\Omega$, $Z_{3o} = 81\,\Omega$, $Z_4 = 92\,\Omega$, - - - - with $Z_1 = 96\,\Omega$, $Z_{2e} = 160\,\Omega$, $Z_{2o} = 77\,\Omega$, $Z_{3e} = 101\,\Omega$, $Z_{3o} = 80\,\Omega$, $Z_4 = 90\,\Omega$.

In the following microstrip examples, a practical substrate with the relative dielectric constant of 3.48 and the height of $0.762\,\mathrm{mm}$ is applied. Fig. 7 shows the physical dimension definition of the final layout of this fabricated bandstop filter. The operating center frequency of this fabricated bandstop filter is $3\,\mathrm{GHz}$. This bandstop filter uses the following physical dimension values: $L0 = 7\,\mathrm{mm}$ ($50\,\mathrm{Ohm}$ microstrip line of input and output ports), $W0 = 1.69\,\mathrm{mm}$, $L1 = 18\,\mathrm{mm}$, $W1 = 0.4\,\mathrm{mm}$, $L2 = 16.23\,\mathrm{mm}$, $W2 = 0.3\,\mathrm{mm}$, $S2 = 0.83\,\mathrm{mm}$, $L3 = 15.92\,\mathrm{mm}$, $W3 = 0.44\,\mathrm{mm}$, $S3 = 1.2\,\mathrm{mm}$, $L4 = 15\,\mathrm{mm}$, $W4 = 1.8\,\mathrm{mm}$, $L5 = 16.4\,\mathrm{mm}$ (impedance matching microstrip line of input and output ports), $W5 = 0.3\,\mathrm{mm}$. Fig. 8 shows the practical
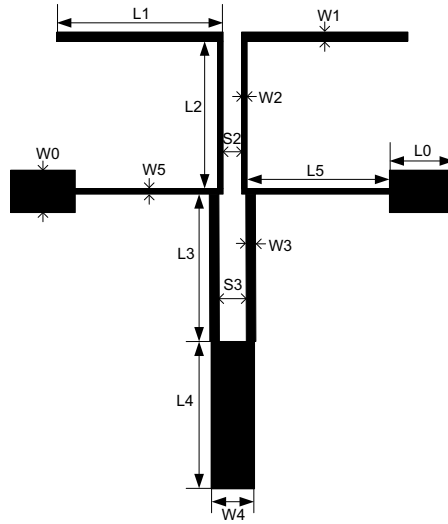
Figure 7. The physical dimension definition of the proposed microstrip bandstop filter.

photograph of the final fabricated microstrip bandstop filter.

A microstrip line being quasi TEM in nature, θ_0 is always less than θ_e. As a consequence, the number of zeros may decrease, in the worst case to two. $\theta_e = \theta_0$ can be achieved by cutting rectangular grooves along the inside edges of the coupled-lines. The dimensions of the grooves can be obtained by using a full wave simulator. Here, two 2.5 mm × 0.1 mm and 2.0 mm × 0.2 mm rectangular grooves are used to obtain $\theta_e = \theta_0$, as shown in Fig. 8. The simulated results shown in Fig. 9 is accomplished by a full-wave simulation tool while the measurement is performed by using Agilent N5230C network analyzer. Compared with the simulated results, the location of transmission zeros deviates slightly from the center frequency. This problem is mainly attributed to the substrate, radiation, dielectric loss, the fabricated tolerance and the machined accuracy. Similarly, we can observe that the number of transmission zeros decreases to three. The grooves on the inner sides of the lines result in a stepped impedance line that reduces the number of zeros to three. This problem can be avoided by increasing the number of the grooves while keeping their dimensions small to obtain $\theta_e = \theta_0$. Nevertheless, the full-wave simulated and measured scattering parameters are in good agreement. The measured 20 dB bandstop fractional bandwidth is about 94% (1.32 GHz–4.14 GHz). The attenuation rate at the
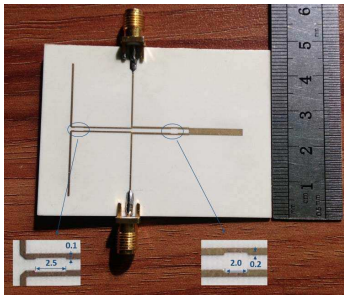
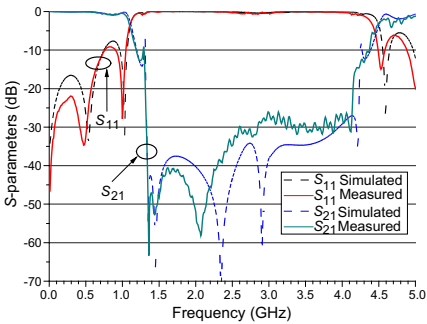**Figure 8.** The photograph of the fabricated microstrip bandstop filter.

Figure 9. The simulated and measured results of filter (the operating frequency is 3 GHz).

Table 2. Comparison of the BSF performances.

Ref.	f_0 (GHz)	20 dB FBW(%)	Attenuation slope Lower (dB/GHz)	Attenuation slope Upper (dB/GHz)	Lower passband IL (dB)
[12]	1.5	122.5	227.9	123.2	< 1
[16]	1.5	98.5	215.1	117.6	< 1
[18]	1.5	65.3	–	–	< 1
[19]	2.6	< 92	–	–	< 2
[21]	6	< 100	–	–	< 1
This work	3	94	320	208.75	< 1

FBW = Fractional Bandwidth, IL = Insertion Loss.

passband to stopband transition knee on the lower side of the stopband is 320 dB/GHz (attenuation: 12.2 dB at 1.30 GHz and 50.6 dB at 1.42 GHz), while on the upper side of the stopband it is 208.75 dB/GHz (attenuation: 31.2 dB at 4.12 GHz and 14.5 dB at 4.2 GHz). The lower 9 dB return-loss pass-band is from DC to 1.05 GHz while the upper 9 dB return-loss pass-band is from 4.55 to 5 GHz. The lower pass-band insertion loss is within 1 dB up to 1.04 GHz. The measured group-delay variation in the lower pass-band of DC-1.2 GHz is less than 1.6 ns, and in the upper pass-band of 4.2–6.0 GHz less than 3.6 ns, as shown in Fig. 10. Table 2 shows the comparison of the proposed filter with other reported wideband BSFs [12, 16, 18, 19, 21]. The proposed filter shows a wide stopband with sharp skirt selectivity, low insertion loss.
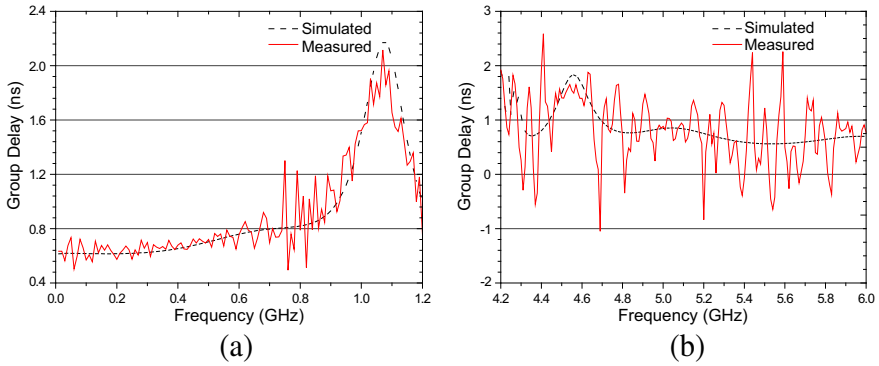
Figure 10. The simulated and measured group delay of the bandstop filter. (a) With lower pass-band from DC-1.2 GHz, (b) with upper pass-band from 4.2–6 GHz.

5. CONCLUSIONS

A novel circuit configuration is proposed to construct a compact, sharp-rejection, wideband bandstop filter (BSF). This proposed circuit configuration includes two-section coupled lines and three open-circuit transmission-line stubs. The rigorous theoretical analysis and complete numerical simulation are discussed. The demonstrated reflection and transmission zeros character may be helpful to guide the synthesis of this proposed BSF. Four numerical examples and one fabricated microstrip BSF verify our proposed idea. The measured results show a good agreement with predicted performance. This BSF has several advantages including compact size, analytical scattering parameters, wide stopband, sharp-rejection, good group delay, easy implementation and avoiding any lumped elements.

ACKNOWLEDGMENT

REFERENCES

1. Hong, J.-S. and M. J. Landcaster, *Microstrip Filters for RF/Microwave Applications*, Chapter 2, Wiley, New York, 2001.

2. Chen, H., Y.-H. Wu, Y.-M. Yang, and Y.-X. Zhang, "A novel and compact bandstop filter with folded microstrip/CPW hybrid structure," *Journal of Electromagnetic Waves and Applications*, Vol. 24, No. 1, 103–112, 2010.

3. Matthaei, G. L., L. Oung, and E. M. T. Jones, *Microwave Filters, Impedance Matching Networks and Coupling Structures*, McGraw Hill, New York, 1964.

4. Pozar, D. M., *Microwave Engineering*, 2nd Edition, Wily, New York, 1998.

5. Wu, Y., Y. Liu, S. Li, and C. Yu, "A simple microstrip bandpass filter with analytical design theory and sharp skirt selectivity," *Journal of Electromagnetic Waves and Applications*, Vol. 25, Nos. 8–9, 1253–1263, 2011.

6. Yu, W.-H., J.-C. Mou, X. Li, and X. Lv, "A compact filter with sharp-transition and wideband-rejection using the novel defected ground structure," *Journal of Electromagnetic Waves and Applications*, Vol. 23, Nos. 2–3, 329–340, 2009.

7. Wu, Y., Y. Liu, S. Li, and C. Yu, "A new wide-stopband low-pass filter with generalized coupled-line circuit and analytical theory," *Progress In Electromagnetics Research*, Vol. 116, 553–567, 2011.

8. Gómez-García, R. and J. I. Alonso "Design of sharp-rejection and low-loss wide-band planar filters using signal-interference techniques," *IEEE Microw. Wireless Compon. Lett.*, Vol. 15, No. 8, 530–532, Aug. 2005.

9. Sánchez-Soriano, M. A., E. Bronchalo, and G. Torregrosa-Penalva, "Compact UWB bandpass filter based on signal interference techniques," *IEEE Microw. Wireless Compon. Lett.*, Vol. 19, No. 11, 692–694, Nov. 2009.

10. Hong, J.-S. and M. J. Lancaster, "Design of highly selective microstrip bandpass filters with a single pair of attenuation poles at finite frequencies," *IEEE Trans. on Microw. Theory and Tech.*, Vol. 48, No. 7, 1098–1107, Jul. 2000.

11. Lee, H.-M. and C.-M. Tsai, "Improved coupled-microstrip filter design using effective even-mode and odd-mode characteristic impedances," *IEEE Trans. on Microw. Theory and Tech.*, Vol. 53, No. 9, 2812–2818, Sep. 2005.

12. Velidi, V. K. and A. B. Guntupalli, "Sharp-rejection ultra-wide bandstop filters," *IEEE Microw. Wireless Compon. Lett.*, Vol. 19,

No. 8, 503–505, Aug. 2009.

13. Schiffman, B. and G. Matthaei, "Exact design of band-stop microwave filters," *IEEE Trans. on Microw. Theory and Tech.*, Vol. 12, No. 1, 6–15, Jan. 1964.

14. Horton, M. and R. Menzel, "General theory and design of optimum quarter wave TEM filters," *IEEE Trans. on Microw. Theory and Tech.*, Vol. 13, No. 5, 316–327, May 1965.

15. Mandal, M. K. and S. Sanyal, "Compact bandstop filter using signal interference technique," *Electron. Lett.*, 110–111, Jan. 2007.

16. Divyabramham, K., M. K. Mandal, and S. Sanyal, "Sharp-rejection wideband bandstop filters," *IEEE Microw. Wireless Compon. Lett.*, Vol. 18, No. 10, 662–664, Oct. 2008.

17. Mandal, M. K., K. Divyabramham, and V. K. Velidi, "Compact wideband bandstop filter with five transmission zeros," *IEEE Microw. Wireless Compon. Lett.*, Vol. 22, No. 1, 4–6, Jan. 2012.

18. Mandal, M. K., K. Divyabramham, and S. Sanyal, "Compact, wideband bandstop filters with sharp rejection characteristic," *IEEE Microw. Wireless Compon. Lett.*, Vol. 18, No. 10, 665–667, Oct. 2008.

19. Cui, D., Y. Liu, Y. Wu, S. Li, and C. Yu, "A compact bandstop filter based on two meandered parallel-coupled lines," *Progress In Electromagnetics Research*, Vol. 121, 271–279, 2011.

20. Wu, Y. and Y. Liu, "A coupled-line band-stop filter with three-section transmission-line stubs and wide upper pass-band performance," *Progress In Electromagnetics Research*, Vol. 119, 407–421, 2011.

21. Hsieh, M.-Y. and S.-M. Wang, "Compact and wideband microstrip bandstop filter," *IEEE Microw. Wireless Compon. Lett.*, Vol. 15, No. 7, 472–474, Jul. 2005.